Large thermoelectric effects in p-SiC/p-Si and n-SiC/p-Si heterojunctions

Pablo Guzman [a,*], Toan Dinh [a,b], Thanh Nguyen [a,b], Abu Riduan Md Foisal [a], Hung Nguyen [a], Quan Nguyen [a], Tuan-Khoa Nguyen [a], Hoang-Phuong Phan [a], Philip Tanner [a], Peter Woodfield [c], Van Thanh Dau [c], Huaizhong Li [c], Nam-Trung Nguyen [a], Dzung Viet Dao [a,c]

[a] Queensland Micro- and Nanotechnology Centre, Griffith University, Queensland, Australia
[b] University of Southern Queensland, Queensland, Australia
[c] School of Engineering and Built Environment, Griffith University, Queensland, Australia

ABSTRACT

The thermoelectric effect is important for thermal sensing, energy harvesting and other applications. This paper investigates the Seebeck coefficient of silicon carbide (SiC) on silicon (Si) heterojunctions and discusses the mechanism underlying the observed effects. The measured Seebeck coefficients of p-3C-SiC/p-Si and n-3C-SiC/p-Si heterojunctions are much higher than other reported values for SiC materials. The maximum Seebeck coefficients of p-3C-SiC/p-Si and n-3C-SiC/p-Si obtained were 1720 μV/K at 383 K and –421 μV/K at 396 K, respectively. These values are almost three times higher than those of other p-SiC and n-SiC materials. The high Seebeck coefficient in SiC/Si heterojunctions is attributed to the unique structure of the heterojunctions, which enables thermally activated charge carriers to migrate from Si to SiC. The results suggest that these heterojunctions can be exploited to develop highly sensitive self-powered thermal sensors.

1. Introduction

Silicon (Si) is the dominant material for fabricating micromechanical components and microelectronics [1]. Because Si is the most commonly used material, fabrication technology has evolved around Si production. However, Si yet exhibits a small band gap that can compromise its reliability and functionality when subjected to increased temperature. Thus, many other semiconductors with higher band gaps have emerged as possible replacements for application in harsh environments, such as silicon carbide (SiC), gallium nitride and gallium arsenide.

As a possible Si replacement, SiC possesses excellent mechanical and electrical properties, a wide band gap, extraordinary chemical inertness, mechanical robustness and a high-temperature stability [2–5]. Additionally, 3C-SiC growth can be performed on an Si substrate, allowing compatibility with the traditional microfabrication process and reducing production cost. Therefore, the development of position-sensitive detectors [6], mechanical sensors [7,8], diodes [9,10] and high-frequency electronics [11] based on the 3C-SiC/Si heterojunction has gained increasing interest.

For thermal applications, the thermoelectric properties of SiC and Si have been extensively studied. SiC particles have been used to enhance the Seebeck effect in different materials [12–14]. Additionally, α-SiC

demonstrated a maximum value of 600 μV/K, while a low-doped p-type SiC reached a value of 300 μV/K. The thermoelectric properties of SiC nanowires have been studied at the nanoscale level [15], while SiC thin films have also attracted attention [16]. For instance, heavily doped n-type polycrystalline SiC thin film with a Seebeck value of –20 μV/K has been reported [17]. Further, other research has studied the Seebeck coefficient of monocrystalline and polycrystalline SiC measured at 300–533 K [18]. Yamashita revealed a Seebeck coefficient value of –198 μV/K for n-type Si [19] and –130 μV/K for n-type polysilicon [20]. P-type poly-Si and Si ingots have indicated Seebeck coefficients of 300 μV/K [21] and 411 μV/K, respectively [22]. Despite these existing studies, how the SiC/Si heterojunction contributes to the Seebeck effect has not yet been reported.

In this paper, we fabricated 3C-SiC/Si heterojunctions by growing single crystalline p-3C-SiC and n-3C-SiC nanofilms on p-Si substrate using a low-pressure chemical vapor deposition (LPCVD) process. Some preliminary results related to the n-SiC/p-Si heterojunction have been published previously [23]. This work will advance the study by [23] through proposing a more thorough explanation of the mechanisms behind the large Seebeck coefficient and its dependence on the temperature of both p-3C-SiC/p-Si and n-3C-SiC/p-Si heterojunctions. This is done through considering the activation energies of acceptor atoms in
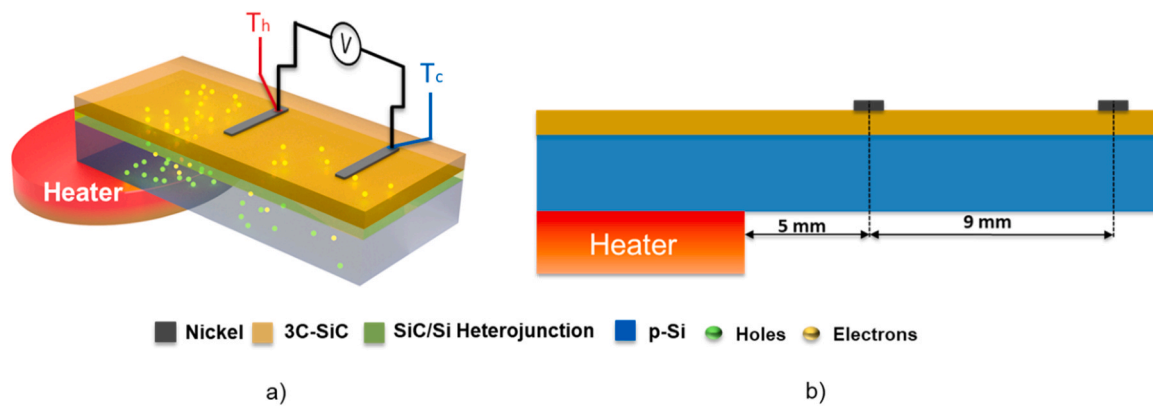
Fig. 1. a) Schematic diagram for measuring the Seebeck coefficients of p-3C-SiC/p-Si and n-3C-SiC/p-Si heterojunctions; b) Dimensions of the SiC/Si device are 35 mm × 6.5 mm × 0.63 mm (length × width × thickness) and dimensions of Ni electrode 3400 μm × 300 μm × 0.3 μm (length × width × thickness).
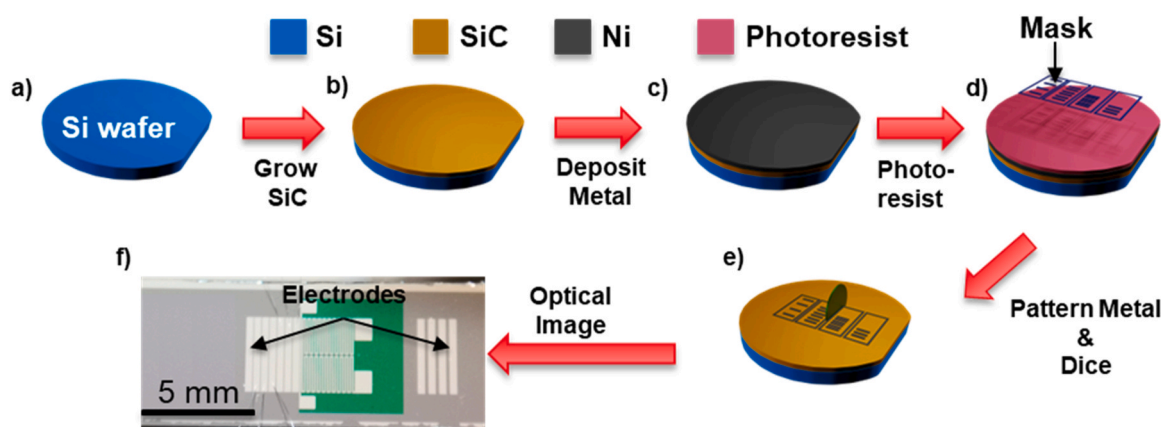

Fig. 2. Fabrication process of the n-3C-SiC/p-Si and p-3C-SiC/p-Si heterojunctions: a) p-Si wafer, b) growth of n-3C-SiC or p-3C-SiC on p-Si wafer, c) Sputtering of Ni layer, d) deposition of photoresist, photolithography and Ni etching, e) Dicing. f) Optical image of the device.

p-3C-SiC, p-Si, and donor atoms in n-3C-SiC to explain the behaviour of the Seebeck coefficient at different temperatures. The maximum point of the n-3C-SiC/p-Si Seebeck coefficient was also discussed. The Seebeck coefficient was measured in an extended range of temperatures between 336 K to 434 K. The maximum Seebeck coefficients in the p-3CSiC/p-Si and n-3C-SiC/p-Si heterojunctions were measured to be 1720 μV/K and −421 μV/K, respectively. Overall, the Seebeck values reported in this study are almost three times higher than those previously reported for SiC materials. These high values together with steep temperature gradients can open the door for developing new self-powered thermal sensors. Moreover, because of differences in nonlinearity with absolute temperature between the two pairs of materials, using both p-SiC/p-Si and n-SiC/p-Si heterojunctions together in one sensing unit could potentially extract the absolute temperature and not just a temperature difference using the Seebeck effect.

2. Design and Fabrication of SiC/Si Heterojunction

Fig. 1a shows the schematic sketch of the proposed p-3 C-SiC/p-Si and n-3 C-SiC/p-Si heterojunctions devices for the characterization of the Seebeck coefficient. The thickness of p-Si was 600 μm and those for p-3 C-SiC and n-3 C-SiC films were 390 nm. The distance between the two electrodes is 9 mm. Two thermocouples were attached to the two electrodes (labeled as T_h and T_c, for hot and cold electrodes) to simultaneously measure temperatures at each electrode. The device is attached to a Linkam HFS600 heater and positioned at a distance of 5 mm from the left electrode (Fig. 1b). The temperature of the hot electrode was accurately controlled from 336 to 434 K by the heater. The

non-uniform thermal energy applied to the system excites charge carriers in Si and SiC layers, inducing a gradient of charge carrier concentration, and hence a voltage between the two electrodes. The Seebeck coefficient is obtained by the ratio of the voltage and the temperature difference between the two electrodes:

$$S = \frac{V}{\Delta T} = \frac{V}{(T_h - T_c)} \tag{1}$$

where V and ΔT are respectively the potential and temperature differences between the hot electrode and cold electrode.

A single-crystal 6-inch lightly doped (10^{14} cm^{-3}) p-type Si (100) wafer was used as the substrate (Fig. 2a). N-type and p-type 3C-SiC (100) films were epitaxially grown on the p-type Si substrate using a low-pressure chemical vapor deposition (LPCVD) reactor at 1000 °C, (Fig. 2b). C_3H_6 and SiH_4 were used as precursors to supply carbon and silicon atoms [24]. For n-type and p-type doping, ammonia (NH_3) and trimethylaluminum [$(CH_3)_3Al$] were used, respectively. The doping concentrations of p-SiC and n-SiC were measured by the four-point probe measurement method to be approximately 10^{18} cm^{-3} and 10^{19} cm^{-3}, respectively. Next, a 300-nm thick nickel film was sputtered on the surface of the 3C-SiC thin film (Fig. 2c). Photoresist AZ1512 (~4 μm) was spin-coated on top of the 3C-SiC (Fig. 2d). Electrodes were patterned by using the maskless aligner Heidelberg MLA150 to define the electrode shape on the photoresist, and then nickel was etched to form nickel electrodes. Finally, the samples were cleaned and diced (Fig. 2e). Fig. 2f shows an optical image of the fabricated sample.
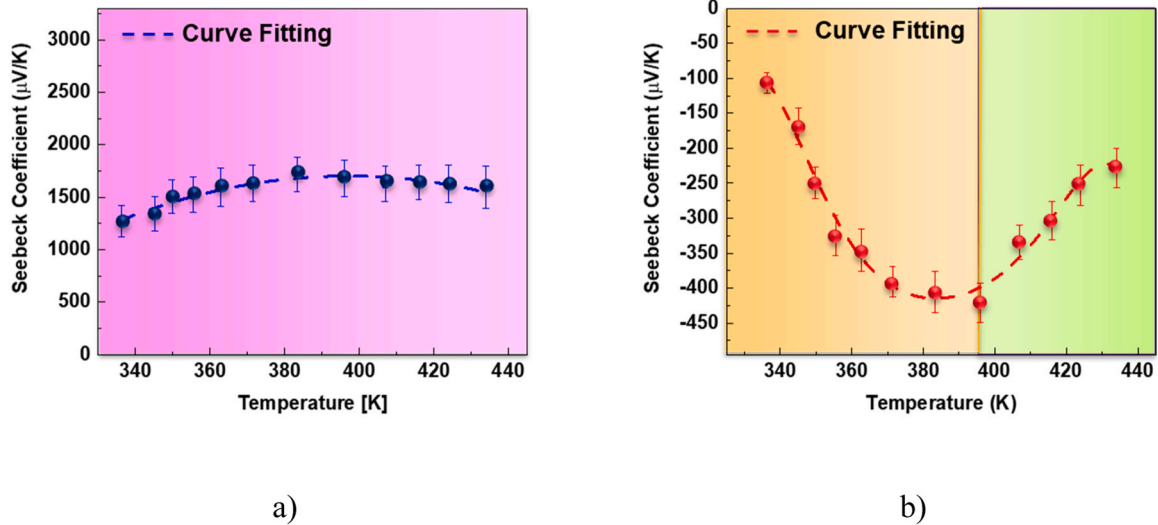
a)

b)

Fig. 3. Seebeck coefficient vs temperature of the hot electrode for a) p-3C-SiC/p-Si heterojunction and b) n-3C-SiC/p-Si heterojunction.

3. Results and discussion

The stability of temperature is a critical parameter for performing a reproducible and consistent measurement of the Seebeck coefficient. Fig. 1 shows our experimental setup, which induces a temperature range (336 K to 434 K) for the hot electrode T_h to measure the Seebeck coefficient of the p-3C-SiC/p-Si and n-3C-SiC/p-Si heterojunctions at various temperatures. The temperature difference between the top and bottom of the samples was measured to be from 7 K to 30 K, while the temperature difference between the hot and cold electrode ranged from 5 K to 9 K. Heat losses can explain the above temperature differences which arise due to heat transfer via free convection and radiation into the surroundings, which are at ambient temperature.

The voltage was measured between the hot and cold electrodes and the Seebeck coefficient was calculated using Eq. 1. The measurement

was carried out three times for each condition which are shown in Fig. 3. The p-3C-SiC/p-Si device indicated a positive Seebeck coefficient while the n-3C-SiC/p-Si device indicated a negative Seebeck coefficient. These positive and negative signs align with the literature. Because the charge carriers determine the magnitude and sign of the Seebeck coefficient, holes, as the majority charge carrier in p-3C-SiC determined a positive value [25], while electrons, as the majority charge carrier in n-3C-SiC determined a negative value [26]. For the p-3C-SiC/p-Si sample, the maximum Seebeck coefficient was 1720 μV/K at 386 K as shown in Fig. 3a. On the other hand, the n-3C-SiC/p-Si showed a maximum Seebeck coefficient of −421 μV/K at 396 K as shown in Fig. 3b. For the temperature range considered, the Seebeck coefficient for p-3C-SiC/p-Si appears to be more stable than that for n-3C-SiC/p-Si.

The results in Fig. 3 can be explained in terms of how the charge carriers are generated in the heterojunctions when thermal energy is

Table 1
Temperatures of the samples and associated charge carrier generation in n-3C-SiC, p-Si, p-3C-SiC.

Temperature	Thermal energy (kT)	Activation energy dopants	Fully ionized atom	Band diagram
T_h: 336 K T_{Si}: 343 K	28.9 meV 29.6 meV	Nitrogen: 15 meV	Nitrogen donor in n-SiC	
T_h: 396 K T_{Si}: 416 K	34.1 meV 36 meV	Boron: 36 meV	Boron acceptor in p-Si	
T_h: 434 K T_{Si}: 464 K	38 meV 40 meV	Aluminum: 45 meV	Aluminum acceptor in p-SiC	

Note: T_h and T_{Si} is the temperature at the hot electrode and in p-Si layer, thermal energy is calculated from (kT) at each location. $E_{c,SiC}$ = Conduction band of SiC, $E_{V,SiC}$ = Valence band of SiC, $E_{D,N}$= Donor level of nitrogen in SiC, $E_{A,Al}$= Acceptor level of aluminum in SiC, $E_{c,Si}$=Conduction band of Si, $E_{V,Si}$=Valence band of Si and $E_{A,B}$=Acceptor level of boron in Si.
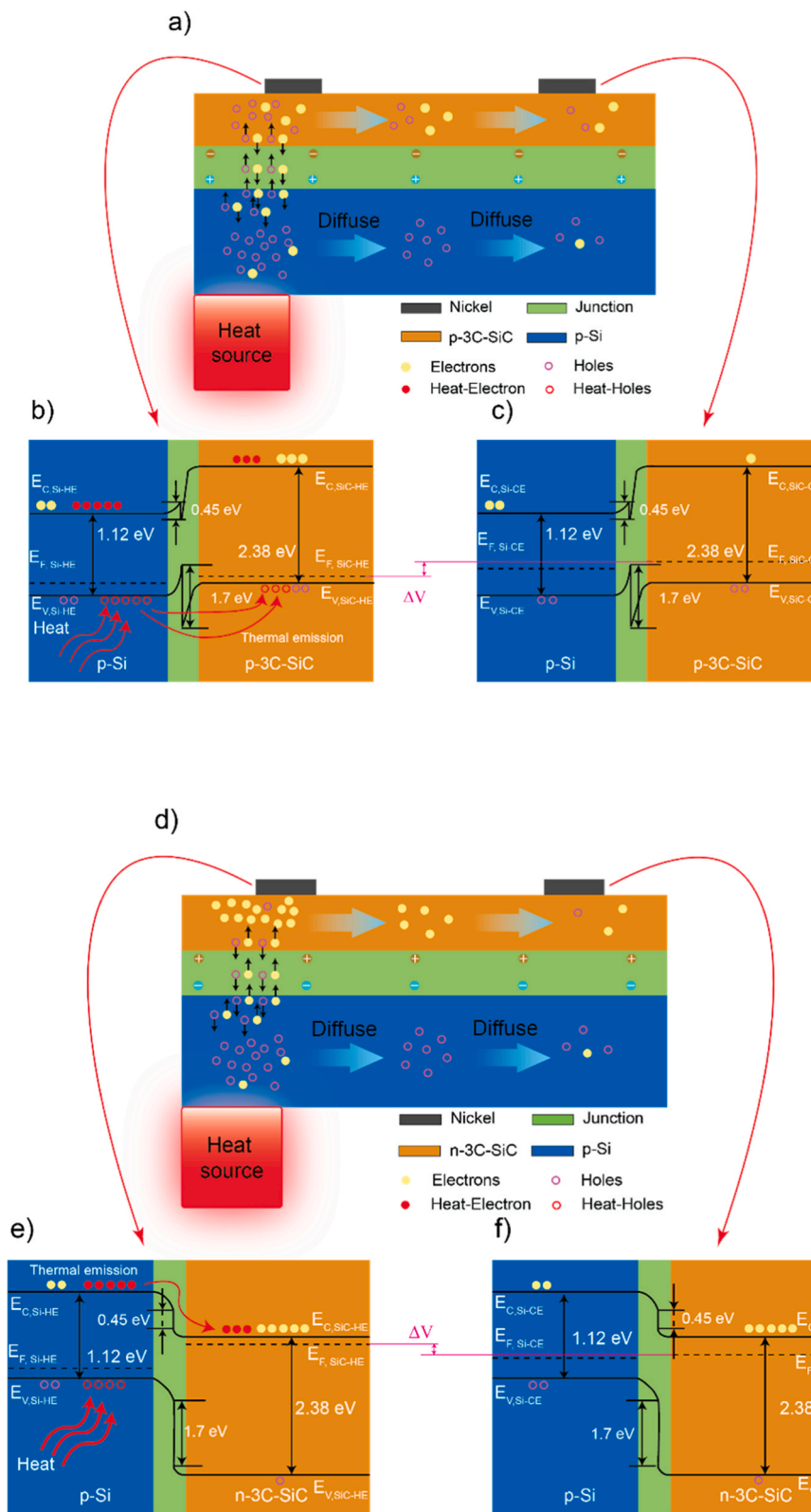
Fig. 4. a) p-3C-SiC/p-Si structure; b) Band diagram for the hot electrode; c) Band diagram for the cold electrode; d) n-3C-SiC/p-Si structure; e) Band diagram for the hot electrode; f) Band diagram for the cold electrode.

introduced to the material. If this energy is higher than the activation energy of the impurities or the energy gap of intrinsic Si or SiC, the charge carriers will be fully generated. Specifically, in p-Si and p-3 C-SiC, the charge carrier concentration is proportional to exp(-E_a/kT), where E_a is the activation energy of the acceptor, k is the Boltzmann constant (k= 8.6174×10^{-5} eV/K), and T is the temperature (K). The activation energy of the acceptor in p-Si (boron) is approximately 36 meV [27]. While the activation energy of the acceptor in p-3 C-SiC (aluminum) is 160 meV [25] which decreases to 45 meV for higher doping concentrations [28]. Similarly, in n-3 C-SiC, the charge carrier

concentration produced by the thermal energy is proportional to exp $(-E_d/kT)$, where E_d is the activation energy of the donor. The activation energy of the donor n-3 C-SiC (nitrogen) is 50 meV for low doping concentration which decreases to 15 meV for high doping concentration [29–31]. The charge carrier concentrations generated from Si and 3 C-SiC atoms by thermal energy are proportional to exp($-E_g/2kT$), where E_g is the band gap, $E_g = 2.38$ eV and = 1.12 eV for 3 C-SiC and Si, respectively. At temperatures below 500 K as in this work, the contributions of the intrinsic Si and SiC are so small compared to that of the impurities [32] that they can be considered negligible. Table 1 illustrates the charge carriers generated from impurities at different temperatures at which impurities (nitrogen, boron, aluminum) are fully ionized.

The charge carriers generated in Si will move to SiC due to the built-in electric field across the SiC/Si heterojunctions (Fig. 4a and 4d). For p-3C-SiC/p-Si (Fig. 4a) the majority of charge carriers migrating to SiC are holes while for n-3C-SiC/p-Si (Fig. 4d) the majority are electrons. The thermal energy induces a higher charge carrier concentration near the hot electrode compared to the cold electrode. Fig. 4a and d illustrate the gradient of charge carrier concentration between the two electrodes for p-3C-SiC/p-Si and n-3C-SiC/p-Si, respectively. This results in a potential difference between the two electrodes.

Fig. 4b, c, e, and f illustrate the band diagrams of the SiC/Si heterojunctions at the hot and cold electrodes. This is based on the conduction band offsets between the conduction bands and valence bands of Si and SiC. Specifically, the conduction band offset $\Delta E_C = 0.45$ eV and the valence band offset $\Delta E_V = 1.7$ eV [33,34]. Considering the charge carrier concentration for the p-3 C-SiC/p-Si in the hot electrode, the Fermi energy level of p-Si ($E_{F\text{-Si-HE}}$) moves closer to the valence band of Si. Similarly, the Fermi energy level of the p-3C-SiC ($E_{F\text{-SiC-HE}}$) is closer to valence band of SiC, Fig. 4b. While near to the cold electrode, the Fermi energy levels for p-Si ($E_{F\text{-Si-CE}}$) and p-SiC ($E_{F\text{-SiC-CE}}$) are levelled and are located further from the valence bands compared with the levels for the hot electrode (Fig. 4c). In the Si region closer to the hot electrode, charge carriers (holes) with enough energy can migrate from the p-Si to the p-3C-SiC through thermal emission, tunnelling and built-in electric field across the p-3C-SiC/p-Si heterojunction (Fig. 4a, b), then diffuse towards the cold electrode (Fig. 4a). A potential difference is generated between the electrodes because of the gradient of charge carrier concentration. This potential difference increases as the temperature rises because heat energy activates more charge carriers in the region under the hot electrode.

Similarly, near to the hot electrode in the n-3C-SiC/p-Si, electron hole pairs are generated, and electrons migrate to SiC due to the built-in electric field across the heterojunction. More holes are left behind in p-Si. Therefore, the Fermi energy level of the p-Si ($E_{F\text{-Si-HE}}$) moves closer to the valence band, while the Fermi energy level of the n-3C-SiC ($E_{F\text{-SiC-HE}}$) moves closer to the conduction band (Fig. 4e). For the region near to the cold electrode, Fermi levels are further away from the band edges compared to the hot electrode (Fig. 4f). A potential difference between hot and cold electrodes arises as a result of a charge carrier concentration gradient between the hot and cold electrodes.

The Seebeck coefficient for p-3 C-SiC/p-Si is more stable than that for n-3C-SiC/p-Si as shown in Fig. 3. The stability of p-3C-SiC/p-Si is attributed to the high thermal energy required to fully ionize the aluminum acceptors in p-3 C-SiC (activation energy of aluminum is 45 meV). Close to room temperature and with the increasing temperature to 383 K, boron acceptor in p-Si is the main contributor to the generation of charge carriers. At temperatures above 396 K, p-Si acceptors have been fully activated and no longer contribute to the gradient of charge carriers. Nonetheless, the acceptors in p-3 C-SiC sustains the contribution of charge carriers because the thermal energy is insufficient to reach full ionization. On the other hand, the Seebeck coefficient for n-3 C-SiC/p-Si changes rapidly with temperature and it has a maximum at 396 K. Table 1 shows how charge carriers are generated at different temperatures. For n-3C-SiC/p-Si, close to room

temperature the thermal energy is enough to ionize nitrogen donors in n-3 C-SiC (activation energy of nitrogen is 15 meV), and electrons are generated in n-3 C-SiC. When temperature increases further, boron acceptors in p-Si generate charge carriers and more electrons will move from p-Si to n-3 C-SiC. Therefore, higher charge carrier concentration occurs near the hot electrode resulting in a higher potential difference between the two electrodes and a higher Seebeck coefficient. The n-3 C-SiC/p-Si heterojunction shows a saturation point at $T_h = 396$ K in Fig. 3b (or $T_{Si} = 416$ K in Si, Table 1). The saturation point exists because the thermal energy has already exceeded the activation energy of nitrogen (15 meV) and reached the activation energy of boron (36 meV - see Table 1), therefore further increases in temperature would contribute no more charge carriers near the hot electrode. When temperature of the hot electrode is increased above 396 K (see Fig. 3b and Table 1) the temperature of the cold electrode also increases but initially it is still lower than 396 K, and therefore more charge carriers are still generated near the cold electrode. This results in a decrease of the charge carrier gradient between the two electrodes, thus reducing the potential difference and the Seebeck coefficient.

Fig. 3 shows that the magnitude of the Seebeck coefficient for the p-3C-SiC/p-Si heterojunction is much larger than that of the n-3C-SiC/p-Si heterojunction. This will be explained in the following paragraphs.

The conductivities of a p-type and n-type semiconductors can be expressed by

$$\sigma_p = pe\mu_h \tag{2}$$

and

$$\sigma_n = ne\mu_e \tag{3}$$

where p is the concentration of holes, n is the concentration of electrons, e is charge of an electron 1.602×10^{-19} C, μ_h and μ_e are the mobility of the holes and electrons, respectively. In crystalline semiconductor materials, the mobility is inversely proportional to the effective mass of the drifting charge carriers, i.e. hole effective mass m_h^* and electron effective mass m_e^* [35]. The drift mobilities μ_h and μ_e depend on the mean free times τ_h and τ_e between scattering events via

$$\mu_h = \frac{e\tau_h}{m_h^*} \tag{4}$$

$$\mu_e = \frac{e\tau_e}{m_e^*} \tag{5}$$

where the mean free time τ between scattering events is calculated by [3]

$$\tau = \frac{1}{SV_{th}N_s} \tag{6}$$

where S is the cross-sectional area of the scatter; V_{th} is the mean speed of the electrons (thermal velocity); and N_s is the number of scatters per unit volume of the conductor. The main source of scattering events can be defined as electron-phonon scattering and electron-impurity scattering (ionized donor or acceptor). Because electron-phonon scattering or lattice scattering is dominant at very high temperatures, we consider that electron-impurity scattering is prevalent at temperatures close to room temperature [25]. Close to room temperature, the N_s is small, and the mean free time τ is larger, thus, the drift mobilities μ_h and μ_e are higher.

In the absence of an electric field, the electrons move randomly. Eqs. (4) and (5) show the mobility of holes and electrons depending on the effective mass of the charge carrier. Because the effective mass of the electrons is at least one order of magnitude smaller than the hole effective mass [36], the electrons can move and diffuse faster. In Si, the hole mobility and electron mobility are 471 cm^2/Vs and 1400 cm^2/Vs, respectively [35]. Similarly, at room temperature, the hole mobility in 3C-SiC is 40 cm^2/Vs and the electron mobility is 800 cm^2/Vs [29]. Therefore, the diffusion process of electrons from the hot electrode to

Table 2
Benchmarking of the Seebeck coefficient of different Si and SiC materials.

Authors	Material	Doping type (Concentration)	Temperature range [K]	Seebeck coefficient Min(μV/K)	Seebeck coefficient Max(μV/K)
Zhou et al. [37]	poly-Si	p-type	223 – 573	55	310
Yamashita [19]	Silicon (ingot)	p-type (N/A)	298–576	N/A	411
Huang et al. [20]	Poly Si	p-type	320 – 525	109	145
Yang et al. [38]	Si nanowire	p-type (10^{20} cm^{-3})	300–760	430	550
Ohba et al. [22]	α - SiC	p-type	673–1073	600	500
Cagri et al. [39]	SiC	p-type	323–923	N/A	564
Lei et al. [17]	β -SiC	n-type (10^{20} cm^{-3})	298–573	-10	-20
Kitagawa et al. [40]	β -SiC	n-type (N/A)	673–973	-50	-150
Kitagawa et al. [40]	β -SiC + Si$_3$N$_4$	n-type (N/A)	673–973	-12	-25
Hase et al. [41]	Si -single crystal	n-type (10^{18} cm^{-3})	300–700	-150	-636
Taki et al. [42]	6 H - SiC	n-type	298–973	-70	-200
Hashimoto et al. [43]	Si nanowire	n-type (10^{17} cm^{-3})	293–318	N/A	214
Valentino et al. [15]	β -SiC nanowires	n-type (N/A)	180–370	-40	-65
Our work	n-3 C-SiC/p-Si	n-type (10^{19} cm^{-3})	336–434	-106	-421
Our work	p-3 C-SiC/p-Si	p-type (10^{18} cm^{-3})	336 – 434	1270	1720

the cold electrode is at a higher rate than that of the holes diffusion. As a result, the gradient of charge carriers is higher for the p-3C-SiCp-3 C-SiC in comparison to the n-3C-SiC. Hence, higher potential difference and Seebeck coefficient occurs in p-3C-SiC.

We further benchmark the Seebeck coefficient between this work and other studies that use SiC materials. The results show a significant increase in the Seebeck coefficients of both p- and n-type 3C-SiC/Si heterojunctions even in a lower temperature range, Table 2.

4. Conclusions

This work presented the fabrication of p-3C-SiC/p-Si and n-3C-SiC/p-Si heterojunctions and demonstrated an enhancement of Seebeck coefficients in these structures compared to single SiC materials. Experimental results show large Seebeck coefficients for both p-3C-SiC/p-Si and n-3C-SiC/p-Si heterojunctions with maximum values of 1720 μV/K and -421 μV/K at 383 K and 396 K, respectively. Thermally-induced charge carries, charge carrier transport, and the activation energies of acceptors and donors (aluminum, nitrogen and boron) in p-3C-SiC, n-3C-SiC and p-Si were taken into account to explain the enhancement in the Seebeck coefficients. Also, the mechanism of the thermoelectric effect in the heterojunctions was discussed using energy band diagram. The simple fabrication process and high Seebeck coefficient of p-3C-SiC/p-Si and n-3C-SiC/p-Si heterojunctions show great potential to develop advanced self-powered thermal sensing devices.

CRediT authorship contribution statement

Pablo Guzman: Conceptualization, Investigation, Writing - original draft, Writing - review & editing. **Toan Dinh:** Investigation, Resources, Writing - review & editing. **Thanh Nguyen:** Investigation, Writing - review & editing. **Abu Riduan Md Foisal:** Investigation, Writing - review & editing. **Hung Nguyen:** Methodology, Writing - original draft, Formal analysis. **Quan Nguyen:** Investigation, Resource, Visualization. **Tuan-Khoa Nguyen:** Investigation, Resource, Visualization. **Hoang-Phuong Phan:** Investigation, Methodology, Writing - review & editing. **Philip Tanner:** Investigation, Resource, Visualization. **Peter Woodfield:** Validation, Supervision. **Van Thanh Dau:** Resource, Visualization **Huaizhong Li:** Validation, Supervision. **Nam-Trung Nguyen:** Supervision, Writing - review & editing. **Dzung Viet Dao:** Conceptualization,

Supervision, Writing - review & editing.

Declaration of Competing Interest

The authors declare that they have no known competing financial interests or personal relationships that could have appeared to influence the work reported in this paper.

Data Availability

Data will be made available on request.

Acknowledgments

References

[1] M. Arif, M. Rahman, W.Y. San, A state-of-the-art review of ductile cutting of silicon wafers for semiconductor and microelectronics industries, Int. J. Adv. Manuf. Technol. 63 (5–8) (2012) 481–504, https://doi.org/10.1007/s00170-012-3937-2.

[2] L. Jiang, R. Cheung, A review of silicon carbide development in MEMS applications, Int. J. Comput. Mater. Sci. Surf. Eng. 2 (3–4) (2009) 227–242, https://doi.org/10.1504/IJCMSSE.2009.027484.

[3] A. Elasser, T.P. Chow, Silicon carbide benefits and advantages for power electronics circuits and systems, Proc. IEEE 90 (6) (2002) 969–986, https://doi.org/10.1109/JPROC.2002.1021562.

[4] C.H. Park, B.-H. Cheong, K.-H. Lee, K.J. Chang, Structural and electronic properties of cubic, 2H, 4H, and 6H SiC, Phys. Rev. B 49 (7) (Feb. 1994) 4485–4493, https://doi.org/10.1103/PhysRevB.49.4485.

[5] A.A. Lebedev, Deep level centers in silicon carbide: a review, Semiconductors 33 (2) (2002) 107–130, https://doi.org/10.1134/1.1187657.

[6] H. Nguyen, et al., Effects of photogenerated-hole diffusion on 3C-SiC/Si heterostructure optoelectronic position-sensitive detector, J. Phys. D. Appl. Phys. 54 (26) (2021), https://doi.org/10.1088/1361-6463/abf3ff.

[7] T. Nguyen, et al., Giant piezoresistive effect by optoelectronic coupling in a heterojunction, Nat. Commun. 10 (1) (2019), https://doi.org/10.1038/s41467-019-11965-5.

[8] T. Nguyen, et al., Piezoresistive Effect with a Gauge Factor of 18 »000 in a semiconductor heterojunction modulated by bonded light-emitting diodes, ACS Appl. Mater. Interfaces 13 (29) (2021) 35046–35053, https://doi.org/10.1021/acsami.1c05985.

[9] A. Qamar, D.V. Dao, P. Tanner, H.P. Phan, T. Dinh, S. Dimitrijev, Influence of external mechanical stress on electrical properties of single-crystal n-3C-SiC/p-Si heterojunction diode, Appl. Phys. Express 8 (6) (2015), https://doi.org/10.7567/APEX.8.061302.

[10] P. Tanner, et al., Excellent rectifying properties of the n-3C-SiC/p-Si heterojunction subjected to high temperature annealing for electronics, MEMS, and LED applications, Sci. Rep. vol. 7 (1) (2017) 1–11, https://doi.org/10.1038/s41598-017-17985-9.

[11] A. Acharyya, A. Biswas, P. Das, Introduction to generation, Detect. Process. Terahertz Signals vol. 794 (2022).

[12] N. Farahi, S. Prabhudev, M. Bugnet, G.A. Botton, J.R. Salvador, H. Kleinke, Effect of silicon carbide nanoparticles on the grain boundary segregation and thermoelectric properties of bismuth doped Mg2Si0.7Ge0.3, J. Electron. Mater. vol. 45 (12) (2016) 6052–6058, https://doi.org/10.1007/s11664-016-4892-8.

[13] H. Ju, D. Park, J. Kim, Silicon carbide particles induced thermoelectric enhancement in SnSeS crystal, Funct. Compos. Struct. vol. 1 (1) (2019), https://doi.org/10.1088/2631-6331/ab0c83.

[14] J. Cai, X. Li, Thermoelectric properties of geopolymers with the addition of nano-silicon carbide (SiC) powder, Ceram. Int. 47 (14) (2021) 19752–19759, https://doi.org/10.1016/j.ceramint.2021.03.313.

[15] L.A. Valentín, et al., A comprehensive study of thermoelectric and transport properties of β-silicon carbide nanowires, J. Appl. Phys. 114 (18) (2013), https://doi.org/10.1063/1.4829924.

[16] A. Boyer, E. Cisse, Properties of thin film thermoelectric materials: application to sensors using Seebeck effect, Mater. Sci. Eng. B (1992) 103–111, https://doi.org/10.1016/0921-5107(92)90149-4.

[17] M.I. Lei, M. Mehregany, Characterization of thermoelectric properties of heavily doped n-type polycrystalline silicon carbide thin films, IEEE Trans. Electron Devices 60 (1) (2013) 513–517, https://doi.org/10.1109/TED.2012.2228867.

[18] N. Abu-Ageel, M. Aslam, R. Ager, and L. Rimai, Seebeck coefficient of monocrystalline α-SiC and polycrystalline β-SiC measured at 300–533 K, Semicond. Sci. Technol., 15, 1, pp. 32–33, 2000, doi: 10.1088/0268-1242/15/1/305.

[19] O. Yamashita, Effect of metal electrode on Seebeck coefficient of p- and n-type Si thermoelectrics, J. Appl. Phys. vol. 95 (1) (2004) 178–183, https://doi.org/10.1063/1.1630361.

[20] P. Huang, J. Fu, Y. Lu, J. Liu, J. Zhang, D. Chen, An on-chip test structure to measure the Seebeck coefficient of thermopile sensors, J. Micromech. Microeng. 32 (1) (2022), https://doi.org/10.1088/1361-6439/ac3be1.

[21] X.H. Wang, A. Yamamoto, K. Eguchi, H. Obara, T. Yoshida, Thermoelectric properties of SiC thick films deposited by thermal plasma physical vapor deposition, Sci. Technol. Adv. Mater. 4 (2) (2003) 167–172, https://doi.org/10.1016/S1468-6996(03)00015-9.

[22] Y. Ohba, T. Shimozaki, H. Era, Thermoelectric properties of silicon carbide sintered with addition of boron carbide, carbon, and alumina, Mater. Trans. 49 (6) (2008) 1235–1241, https://doi.org/10.2320/matertrans.MRA2007232.

[23] P. Guzman et al., "Seebeck coefficient in SiC/Si heterojunction for self-powered thermal sensor," in 2021 IEEE Sensors, Oct. 2021, pp. 1–4, doi: 10.1109/SENSORS47087.2021.9639762.

[24] L. Wang, S. Dimitrijev, J. Han, P. Tanner, A. Iacopi, and L. Hold, Demonstration of p-type 3CSiC grown on 150 mm Si(1 0 0) substrates by atomic-layer epitaxy at 1000 °c, J. Cryst. Growth, 329, 1, pp. 67–70, 2011, doi: 10.1016/j.jcrysgro.2011.06.041.

[25] M. Yamanaka, H. Daimon, E. Sakuma, S. Misawa, S. Yoshida, Temperature dependence of electrical properties of n- and p-type 3C-SiC, J. Appl. Phys. 61 (2) (1987) 599–603, https://doi.org/10.1063/1.338211.

[26] J.G. Kim, Y.Y. Choi, D.J. Choi, S.M. Choi, Study on the thermoelectric properties of CVD SiC deposited with inert gases, J. Electron. Mater. 40 (5) (2011) 840–844, https://doi.org/10.1007/s11664-011-1589-x.

[27] W. Scott, C.E. Jones, Infrared spectra of new acceptor levels in boron-doped and gallium-doped silicon, J. Appl. Phys. 50 (11) (1979) 7258–7260, https://doi.org/10.1063/1.325806.

[28] T. Dinh, et al., Thermoresistive properties of p-type 3C-SiC nanoscale thin films for high-temperature MEMS thermal-based sensors, RSC Adv. 5 (128) (2015) 106083–106086, https://doi.org/10.1039/c5ra20289b.

[29] W.J. Moore, Identification and activation energies of shallow donors in cubic SiC, J. Appl. Phys. 1993 (no) (1993), https://doi.org/10.1063/1.354785.

[30] F. Li, et al., Electrical activation of nitrogen heavily implanted 3C-SiC(1 0 0), Appl. Surf. Sci. 353 (2015) 958–963, https://doi.org/10.1016/j.apsusc.2015.06.169.

[31] J.A. Freitas, S.G. Bishop, P.E.R. Nordquist, M.L. Gipe, Donor binding energies determined from temperature dependence of photoluminescence spectra in undoped and aluminum-doped beta SiC films, Appl. Phys. Lett. 52 (20) (1988) 1695–1697, https://doi.org/10.1063/1.99021.

[32] C.D. Thurmond, The standard thermodynamic functions for the formation of electrons and holes in Ge, Si, GaAs, and GaP, J. Electrochem. Soc. 122 (8) (1975) 1133–1141, https://doi.org/10.1149/1.2134410.

[33] T. Dinh, H. Phan, N. Kashaninejad, T. Nguyen, D.V. Dao, N. Nguyen, An On-Chip SiC MEMS device with integrated heating, sensing, and microfluidic cooling systems, Adv. Mater. Interfaces 5 (20) (2018) 1800764, https://doi.org/10.1002/admi.201800764.

[34] A. Qamar, P. Tanner, D.V. Dao, H.P. Phan, T. Dinh, Electrical properties of p-type 3C-SiC/Si heterojunction diode under mechanical stress, IEEE Electron Device Lett. 35 (12) (2014) 1293–1295, https://doi.org/10.1109/LED.2014.2361359.

[35] S.M.Sze and K.K. Ng, Physics of semiconductor devices, Third. New York, 2007.

[36] T. Kimoto and J.A. Cooper, Fundamentals of Silicon Carbide Technology. Singapore: John Wiley & Sons Singapore Pte. Ltd, 2014.

[37] H. Zhou, P. Kropelnicki, J.M. Tsai, C. Lee, Study of the thermoelectric properties of heavily doped poly-Si in high temperature, Procedia Eng. 94 (2014) 18–24, https://doi.org/10.1016/j.proeng.2013.10.011.

[38] L. Yang, D. Huh, R. Ning, V. Rapp, Y. Zeng, Y. Liu, S. Ju, Y. Tao, Y. Jiang, J. Beak, J. Leem, S. Kaur, H. Lee, X. Zheng, R.S. Prasher, High thermoelectric figure of merit of porous Si nanowires from 300 to 700 K., Nat. Commun. 12 (no.) (2021) 6, https://doi.org/10.1038/s41467-021-24208-3.

[39] S. Cagri, O. Kartal, A. Servet, Thermoelectric properties of carbide ceramics: a comparative analysis of thermoelectric properties of - B 4C, SiC and TiC, J. Aust. Ceram. Soc. (0123456789) (2023), https://doi.org/10.1007/s41779-023-00979-4.

[40] H. Kitagawa, N. Kado, Y. Noda, Preparation of N-type silicon carbide-based thermoelectric (pp), Materials 43 (12) (2002) 3239–3241.

[41] M. Hase, D. Tanisawa, K. Kohashi, R. Kamemura, S. Miyake, M. Takashiri, Determination of Seebeck coefficient originating from phonon - drag effect using Si single crystals at different carrier densities, Sci. Rep. 9 (1) (2023), https://doi.org/10.1038/s41598-023-40685-6.

[42] Y. Taki, M. Kitiwan, H. Katsui, T. Goto, Electrical and thermal properties of off-stoichiometric SiC prepared by spark plasma sintering, J. Asian Ceram. Soc. 6 (1) (2018) 95–101, https://doi.org/10.1080/21870764.2018.1446490.

[43] S. Hashimoto, S. Asada, T. Xu, S. Oba, Y. Himeda, R. Yamato, Generator Anomalous Seebeck coefficient observed in silicon nanowire micro thermoelectric generator 023105 (2017), https://doi.org/10.1063/1.4993150.